3D Oncological PET Volume Analysis Using CNN and LVQNN

Mhd Saeed Sharif, Abbes Amira
School of Engineering and Design
Brunel University, West London, United Kingdom
mhd.sharif@brunel.ac.uk

Habib Zaidi
Division of Nuclear Medicine
Geneva University Hospital
CH-1211 Geneva, Switzerland

***Abstract*—The increasing numbers of patient scans and the prevailing application of positron emission tomography (PET) in clinical oncology have led to a need for efficient PET volume handling and the development of new volume analysis approaches to aid clinicians in the diagnosis of disease and planning of treatment. A novel automated system for oncological PET volume segmentation is proposed in this paper. The proposed intelligent system is using competitive neural network (CNN) and learning vector quantisation neural network (LVQNN) for clustering and quantifying phantom and real PET volumes. Bayesian information criterion (BIC) has been used in this system to assess the optimal number of clusters for each PET data set. The experimental study using phantom PET volume was conducted for quantitative evaluation of the performance of the proposed segmentation algorithm. The analysis of the resulting segmentation of clinical oncological PET data seems to confirm that this approach shows promise and can successfully segment patient lesion.**

***Index Terms*—Medical Volume Analysis, Positron Emission Tomography, Tumour, Bayesian Information Criterion.**

I. Introduction

PET volume segmentation is vital for different applications, namely; to correct attenuation effects in PET data-sets and to alleviate artefact introduced through volume reconstruction using tissue component density association [1], for tumour quantification in staging, a process which analyses the development of tumours over time, and to aid in radiotherapy treatment planning [2] [3]. The utilisation of advanced high performance segmentation approaches will be useful in aiding clinicians in diagnosis and radio-therapy planning. Although the task of medical volume segmentation appears simple, the reality is that an in-depth knowledge of anatomy and physiology is required to perform such task on real medical volume. Essentially, the expert observes a particular slice, determines borders between regions and classifies each region. This is commonly completed slice by slice for a 3D volume and requires reslicing procedure of data into the transaxial, sagittal and coronal planes. In addition to this, identifying smaller slice features and contrast modifications are often required. Although, for a typical 3D data-set, the entire expert manual segmentation can take several hours to compute, this approach is perhaps the most reliable and accurate method of medical volume segmentation. This is due to the immense complexity of the human visual system, a system well suited to this task [4] [5] [6] [7].

The main expected challenge of PET modality is the low resolution which is known as a spatial volume effect. This effect should be reduced to the minimum level, so the required information can be precisely extracted from the analysed volume. Analysing and extracting the proper information from PET volumes can be performed by utilising segmentation and classification approaches which provide richer information than that which exists in the original PET volumes alone. The need for accurate and fast analysis for medical volume segmentation leads to exploit artificial intelligence (AI) technologies. ANN is one of the powerful AI techniques that has the capability to learn a set of data and construct weight matrices to represent the learning patterns. The ANN is a mathematical model which emulates the activity of biological neural networks in the human brain.

ANN has great success in many applications including pattern classification, decision making, forecasting, and adaptive control [8]. Many research studies have been carried out in the medical field utilising ANN for medical image segmentation and classification with different medical image modalities. Multilayer perceptron (MLP) neural network have been used in [9] to identify breast nodule malignancy using sonographic images. Multiple classifier system using five neural networks and five sets of texture features extraction for the characterization of hepatic tissue from CT images is presented in [10]. Kohonen self-organising neural network for segmentation and a multilayer backpropagation neural network for classifying multispectral MRI images have been used in [11]. Kohonen neural network also used for image segmentation in [12]. Computer-aided diagnostic (CAD) scheme to detect nodules in lung using multiresolution massive training artificial neural network (MTANN) is presented in [13].

The main objective of this paper is to develop a complete efficient PET volume segmentation system using competitive neural network (CNN) and learning vector quantisation neural network (LVQNN) for clustering and quantifying PET volumes. A statistical approach using Bayesian information criterion (BIC) has been used in this system to choose the optimal number of clusters for each PET data set. The CNN and LVQNN outputs have been evaluated and the best outputs are obtained. Two PET phantom data sets and real PET volumes have been utilised in this study.

This paper is organised as follows. Section II presents theoretical background for the main system components. The proposed medical volume segmentation system is described in section III. Results and analysis are illustrated in section IV, and finally conclusions and future work are presented in section V.

II. Theoretical Background

A. Bayesian information criterion

BIC is employed to approximate the Bayes factor which is consequently used to compare a series of rival theories. BIC is one hypothesis testing approach which uses Bayesian inference. BIC has gained notoriety as a significant approach for model selection and has been used in contexts varying from image processing and analysis [14], to biological and sociological research [15] [16]. Although the BIC does not allow for spatial correlations between voxels to be considered, it does provide a useful strategy for the comparison of contesting models. The model which applied to the data set is denoted by M_K and is defined from the Gaussian distribution utilised and its associated parameters θ_K, where K is a prior number of classes. To compare two competing hypotheses M_K and $M_{K'}$, the posterior

978-1-4244-5309-2/10/$26.00 ©2010 IEEE

probability of each model with voxel labelling Y is computed as follows [15]:

$$p(M_K|Y) = \frac{p(Y|M_K)p(M_K)}{\sum_{l=1}^{K} p(Y|M_l)p(M_l)} \quad (1)$$

$p(M_K)$ is the prior probability of model M_K and in this case the number of clusters considered is taken to be equally likely a priori, therefore:

$$p(M_K) = \frac{1}{K_{\max}} \qquad (K = 1, 2, \ldots, K_{\max}) \quad (2)$$

The ratio of posteriors, $p(Y|M_K)/p(Y|M_L)$, is commonly referred to as the Bayes factor for model M_K versus model M_L. This factor equates to the posterior odds of one hypothesis when the prior probabilities of the two hypotheses are likely to be equal. This also provides a measure of evidential weight provided for the data or against the null hypothesis. $p(Y|M_K)$ represents the integrated likelihood of model M_K rather than the maximised likelihood and is given by:

$$p(Y|M_K) = \int p(Y|\theta_K, M_K)p(\theta_K)d\theta_K \quad (3)$$

$p(Y|\theta_K, M_K)$ is the usual likelihood and $p(\theta_K)$ is the prior assumed to be equally probable for all M_K. Evaluating this integral is combinatorially difficult, however, a good approximation to the integrated likelihood is given by the BIC:

$$BIC = 2\log p(Y|\hat{\theta}_K, M_K) - D_K \log N \quad (4)$$

where $\hat{\theta_K}$ is the maximum likelihood estimator of θ_K obtained from Gaussian mixture fitting:

$$p(Y|\hat{\theta}_K, M_K) = \prod_{i=1}^{N}\sum_{j=1}^{K} \hat{P}_j \Phi_j(Y_i|\hat{\theta}_j) \quad (5)$$

where N is the dimensionality of the data vectors, and D_K is the cardinality of the parameter set employed. The Bayes factor shown in Eq. 6 can be approximated by computing the difference of BIC terms, which are the results of model fitting for different numbers of clusters, K and L [15]:

$$2\log\frac{p(Y|M_K)}{p(Y|M_L)} \approx BIC(K) - BIC(L) \quad (6)$$

Although the absolute value of the BIC is not individually informative due to comparison with the null hypothesis, the disparity between BIC values for competing models provides evidence specifying the use of one model against another.

B. Competitive neural network

CNN consists of a single layer, the N neurons in this competitive layer distribute themselves to recognise frequently presented input vector. The weights are applied to the input vector using negative Euclidean distance approach. The layer's net input is calculated by combining its weighted inputs and biases. CNN is trained using two approaches, the first one is sequential order incremental training which trains the network with weight and bias learning rules with sequential updates. The other approach is random order incremental training which trains a network with weight and bias learning rules with incremental updates after each presentation of an input. Inputs are presented in random order [17].

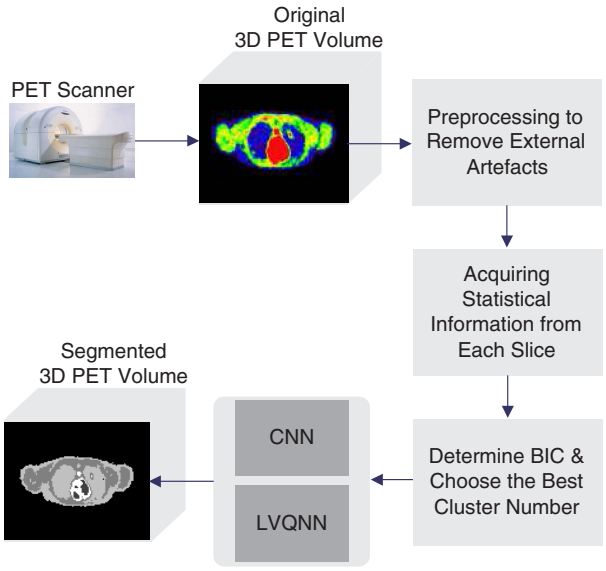

Fig. 1. Proposed system for oncological PET volume segmentation.

C. Learning vector quantisation neural network

LVQNN has two layers, the first layer calculates weighted inputs using negative Euclidean distance approach. The second layer has neurons with purelin activation function, and calculates weighted input using dot product weight approach. There are no biases used in LVQNN. LVQNN is more efficient than CNN in case of large number of inputs. The optimisation procedure implicitly in this network yields the cluster means by estimating optimised assignment for each cluster [18].

III. THE PROPOSED SYSTEM

The proposed medical volume segmentation system is illustrated in Fig. 1. The 3D PET volume acquired from the scanner goes through the preprocessing block, where thresholding, histogram equalisation and median filter are utilised to remove external artefacts and enhance the quality of slices features. Expectation maximization (EM) algorithm is then used to find the maximum likelihood estimation for each cluster in the enhanced volume. The mean, standard deviation, and the probability for each cluster are also calculated. The optimal cluster number is determined using BIC . The processed volume can be then segmented using CNN, and LVQNN, where each voxel is classified into its most likely cluster. The outputs of these approaches are compared in the next step and the best clustered outputs are selected and displayed.

IV. RESULTS AND ANALYSIS

A. Studying PET phantom data

Two PET phantom volumes containing simulated tumours have been utilised in this study. The first data set is obtained from NEMA IEC image quality body phantom which consists of an elliptical water filled cavity with six spherical inserts suspended by plastic rods of volumes 0.5, 1.2, 2.6, 5.6, 11.5, and 26.5 ml. The inner diameters of these spheres are: 10, 13, 17, 22, 28 and 37 mm. The scanner used for acquiring this volume has a resolution of 4.07 mm x 4.07 mm x 5 mm, with voxel volume 0.0828 ml, while the size of the obtained phantom DICOM (digital imaging and communications in medicine) volume is 168 x 168 x 66 [19].

The second data set is Zubal phantom volume, this PET data was simulated using a validated PET Monte Carlo simulation package and consists of two volumes [19]. The first volume contains a raw

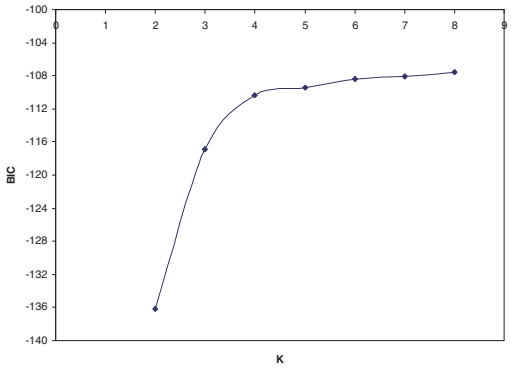

Fig. 2. Plot of BIC values for phantom data set 1, scaled by a factor of 1000.

matrix with isotropic voxels, the size of this volume is 128 x 128 x 180. The second volume contains the same matrix of the first one but without isotropic voxels, it has a size of 128 x 128 x 375. The voxel size in both volumes is 5.0625 mm x 5.0625 mm x 2.4250 mm. The second data sets have 3 tumours in the lungs whose characteristics are given in Table I.

TABLE I
TUMOURS CHARACTERISTICS FOR THE SECOND DATA SET WITH 2 TYPES OF VOXELS

	Isotropic Voxels		Non Isotropic Voxels	
Tumours	Position	Size	Position	Size
1	Slice 68	2 Voxels	Slice 142	2 Voxels
2	Slice 57	3 Voxels	Slice 119	3 Voxels
3	Slice 74	2 Voxels	Slice 155	2 Voxels

To choose the optimal number of clusters for each slice in the processed volume, different values of K have been used. For the proposed application, BIC values are calculated incrementally increasing from $K = 2$ to $K = 8$. K is not further increased, as in this medical application, any additional separation is unnecessary. BIC values tend to increase indefinitely as the number of components increases. An increase in BIC value indicates improved model fit, however, these values typically stabilise on an approximate curve plateau, the beginning of which is usually taken to indicate the optimal K value. The plot of BIC values with K for phantom data set 1 shows that the best K value can be obtained at 4, Fig. 2. For isotropic voxels in phantom data set 2, the optimal cluster number obtained from BIC plot is 5, Fig. 3. For volume with non isotropic voxels in phantom data set 2, the optimal cluster number obtained from BIC plot is also 5 clusters.

The mean, standard deviation, and the probability for each cluster in each slice have been calculated. Table II presents these values for the optimal cluster number for phantom data set 1. Table III shows the statistical information about the best cluster number for phantom data set 2.

An objective evaluation for both neural networks outputs has been performed by comparing the sphere calculated volume with its true (original) volume. CNN and LVQNN have clearly clustered all spheres in phantom data set 1, Fig. 4. Clear segments have been also obtained for phantom data set 2 with isotropic and non isotropic voxels. Due to space limit, Fig. 5 just presents the original and segmented volume for phantom data set 2 with isotropic voxels and tumour 1. Better performance has been achieved using LVQNN than CNN, however the required time for clustering each slice in the processed volume using LVQNN is bigger than the time required for processing each slice using CNN.

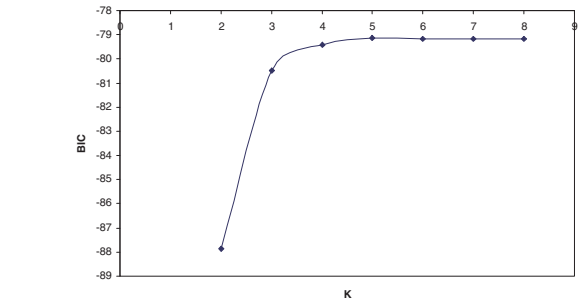

Fig. 3. Plot of BIC values for isotropic phantom data set 2, scaled by a factor of 1000.

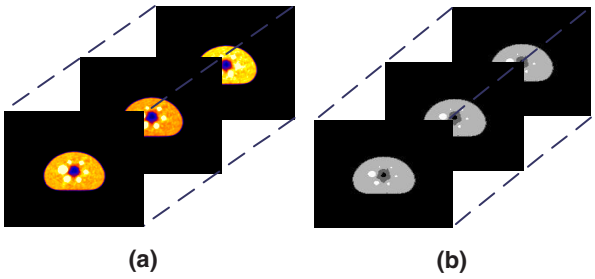

Fig. 4. Phantom data set 1: (a) Original PET volume (168x168x66), (b) segmented volume (168x168x66).

TABLE II
STATISTICAL INFORMATION ABOUT THE BEST CLUSTER NUMBER FOR PHANTOM DATA SET 1

Cluster	Mean	Standard Deviation	Cluster probability
1	1.000986	0.250000	0.469466
2	3.528585	1.602465	0.240734
3	13.024477	7.048304	0.247406
4	57.982584	45.253936	0.042394

TABLE III
STATISTICAL INFORMATION ABOUT THE BEST CLUSTER NUMBER FOR PHANTOM DATA SET 2

Cluster	Mean	Standard Deviation	Cluster probability
1	1.003849	0.250000	0.409114
2	16.288944	6.399162	0.247941
3	26.890255	9.694972	0.197655
4	48.774962	18.579216	0.120429
5	137.468019	57.911212	0.024862

B. Studying real PET volume

The proposed approach has been also tested on real PET volume which contains lung cancer. The optimal cluster number obtained from BIC plot for this data set is 5 clusters, Fig. 6. Table IV shows the statistical information about these clusters. A subjective evaluation based on the clinician knowledge has been carried out for the outputs of the proposed approach. The tumour in these slices has a

maximum diameter on the y-axis of 90 mm (estimated by histology). The segmented tumour has a diameter of 90.18 mm. The segmented volume using the proposed approach has clear detection of ROI as illustrated in Fig. 7.

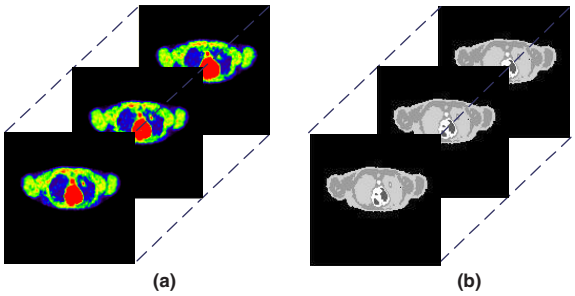

Fig. 5. Phantom data set 2 (Tumour 1): (a) Original PET volume (128x128x180), (b) segmented volume (128x128x180).

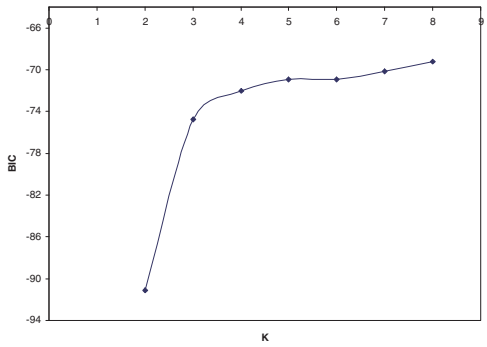

Fig. 6. Plot of BIC values for real PET volume, scaled by a factor of 1000.

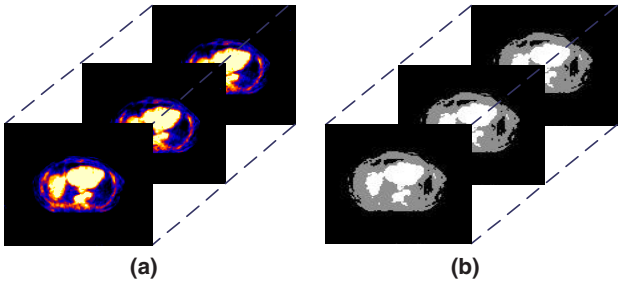

Fig. 7. Real PET data: (a) Original PET volume (128x128x178), (b) segmented volume (128x128x178).

V. CONCLUSIONS AND FUTURE WORK

An intelligent system based on CNN and LVQNN has been proposed for 3D oncological PET volume segmentation. Three PET volume data sets have been used to evaluate the performance of the proposed system. BIC and EM approaches have been used to obtain the optimal cluster number and some statistical information about each slice respectively. Objective and subjective evaluation have been carried out for the system outputs, which has shown promising results. Ongoing research is focusing on the exploitation of other artificial intelligence and feature extraction approaches.

TABLE IV
STATISTICAL INFORMATION ABOUT THE BEST CLUSTER NUMBER FOR REAL PET DATA

Cluster	Mean	Standard Deviation	Cluster probability
1	1.000840	0.250000	0.509741
2	2.911473	1.142062	0.163043
3	9.035780	4.213254	0.146897
4	32.665878	16.455158	0.078470
5	167.509276	52.633532	0.101848

REFERENCES

[1] H. Zaidi, M. Diaz-Gomez, A. Boudraa, and D. O. Slosman. Fuzzy clustering-based segmented attenuation correction in whole-body PET imaging. *Physics in Medicine and Biology*, 47(4):1143–1160, 2002.

[2] I.J. Kalet and M M. Austin-Seymour. Use of medical imagery in the delivery and planning of radiation therapy. *Journal of the American Medical Informatics Association*, 4(5):327–339, 1997.

[3] D. W. G. Montgomery and A. Amira. Automated multiscale segmentation of oncological cerebral MR image volumes. *Proceedings of the IEEE International Conference on Computer Systems and Information Technology*, 2005.

[4] D. A. Mankoff, M. Muzi, and H. Zaidi. *Quantitative analysis in nuclear oncologic imaging*. Springer, 2006.

[5] M. Aristophanous, B.C. Penney, and C.A. Pelizzari. The development and testing of a digital pet phantom for the evaluation of tumor volume segmentation techniques. *Medical physics*, 35(7):3331–3342, 2008.

[6] H. Vees, S. Senthamizhchelvan, R. Miralbell, D.C. Weber, O. Ratib, and H. Zaidi. Assessment of various strategies for ^{18}f-fet petguided delineation of target volumes in high-grade glioma patients. *Eur J Nucl Med Mol Imaging*, 36(2):182–193, 2008.

[7] S. Basu. Selecting the optimal image segmentation strategy in the era of multitracer multimodality imaging: a critical step for imageguided radiation therapy. *Eur J Nucl Med Mol Imaging*, 36(2):180–181, 2009.

[8] G. F. Luger. *Artificial intelligence : structures and strategies for complex problem solving*. Pearson Education Inc., 2009.

[9] S. Joo, W. K. Moon, and H. C.Kim. Computer-aided diagnosis of solid breast nodules on ultrasound with digital image processing and artificial neural network. *Proceedings of the 26th Annual International Conference of the IEEE EMBS*, 2004.

[10] S. G. Mougiakakou, I. Valavanis, K. S. Nikita, A. Nikita, and D. Kelekis. Characterization of CT liver lesions based on texture features and a multiple neural network classification scheme. *Proceedings of the 25' Annual International Conference of the IEEE EMBS*, 2003.

[11] W. E. Reddick, J. O. Glass, E. N. Cook, T. D. Elkin, and R. J. Deaton. Automated segmentation and classification of multispectral magnetic resonance images of brain using artificial neural networks. *IEEE Transactions On Medical Imaging*, 16(6):911–918, December 1997.

[12] C. C. Reyes-Aldasoro and A.L. Aldeco. Image segmentation and compression using neural networks. *Advances in Artificial Perception and Robotics CIMAT*, October 2000.

[13] K. Suzuki, H. Abe, H. MacMahon, and K. Doi. Image-processing technique for suppressing ribs in chest radiographs by means of massive training artificial neural network (MTANN). *IEEE TRANSACTIONS ON MEDICAL IMAGING*, 25(4):406–416, 2006.

[14] Christophe Collet and Fionn Murtagh. Multiband segmentation based on a hierarchical markov model. *Pattern Recognition*, in press.

[15] D. L. Weakliem. A criteque of the bayesian information criterion for model selection. *Sociological Methods and Research*, 27(3):359–397, 1999.

[16] C. T. Volinsky and A. E. Raftery. Bayesian information criterion for censored survival models. *Biometrics*, 56:256–262, 2000.

[17] G. Dreyfus. *Neural Networks Methodology and Applications*. Springer, 2005.

[18] M. A. Arbib. *The handbook of brain theory and neural networks*. Massachusetts Institute of Technology, 2003.

[19] H. Zaidi, F. Schoenahl, and O. Ratib. Geneva PET/CT facility: Design considerations and performance characteristics of two commercial (biograph 16/64) scanners. *Eur J Nucl Med Mol Imaging*, 34, Suppl 2, S166, 2007.